

# Research Articles





How to cite: *Angew. Chem. Int. Ed.* **2022,** *61,* e202204576 International Edition: doi.org/10.1002/anie.202204576 German Edition: doi.org/10.1002/ange.202204576

# A Long-Circulating Vector for Aptamers Based upon Polyphosphodiester-Backboned Molecular Brushes

Yuyan Wang, Dali Wang, Jiachen Lin, Zidi Lyu, Peiru Chen, Tingyu Sun, Chenyang Xue, Mehrnaz Mojtabavi, Armin Vedadghavami, Zheyu Zhang, Ruimeng Wang, Lei Zhang, Christopher Park, Gyu Seong Heo, Yongjian Liu, Sijia S. Dong,\* and Ke Zhang\*

Abstract: Aptamers face challenges for use outside the ideal conditions in which they are developed. These difficulties are most palpable in vivo due to nuclease activities, rapid clearance, and off-target binding. Herein, we demonstrate that a polyphosphodiester-backboned molecular brush can suppress enzymatic digestion, reduce non-specific cell uptake, enable long blood circulation, and rescue the bioactivity of a conjugated aptamer in vivo. The backbone along with the aptamer is assembled via solid-phase synthesis, followed by installation of poly(ethylene glycol) (PEG) side chains using a two-step process with near-quantitative efficiency. The synthesis allows for precise control over polymer size and architecture. Consisting entirely of building blocks that are generally recognized as safe for therapeutics, this novel molecular brush is expected to provide a highly translatable route for aptamer-based therapeutics.

#### Introduction

Aptamers are single-stranded oligonucleotides that can fold into defined secondary structures with a high binding affinity to their targets. [1] Compared to antibodies, aptamers enjoy a wide range of advantages including better production scalability, lower development cost, non-immunogenicity,

[\*] Y. Wang, Dr. D. Wang, J. Lin, Z. Lyu, P. Chen, T. Sun, C. Xue, Z. Zhang, R. Wang, Dr. L. Zhang, C. Park, Prof. S. S. Dong Department of Chemistry and Chemical Biology, Northeastern University Boston, MA 02115 (USA)

E-mail: s.dong@northeastern.edu

M. Mojtabavi, A. Vedadghavami Department of Bioengineering, Northeastern University Boston, MA 02115 (USA)

G. S. Heo, Prof. Y. Liu Department of Radiology, Washington University St. Louis, MO 63110 (USA)

Prof. K. Zhang

Departments of Chemistry and Chemical Biology, Chemical Engineering, and Bioengineering, Northeastern University

Boston, MA 02115 (USA) E-mail: k.zhang@northeastern.edu less susceptibility to biological contamination, better tissue penetration, and greater convenience to develop an antidote. However, these advantages are offset by two serious drawbacks: poor in vivo stability and difficult pharmacological properties (e.g. short blood circulation times, non-specific binding, etc.). As a result, aptamers have seen very limited commercial success, with only one drug on the market: Macugen, a PEGylated, multi-modified aptamer that is delivered locally (intravitreal) to treat agerelated macular degeneration. Even in this space, Macugen is facing severe competition from antibody alternatives (Lucentis or off-label use of Avastin) that bind to the same target, vascular endothelial growth factor A.

Aptamers that bind to a specific target are selected from a random sequence library by a process termed systematic evolution of ligands by exponential enrichment (SELEX).<sup>[6]</sup> Advances in SELEX technologies have enabled a small number of chemical modifications such as 2'-fluoro, 2'amino, and α-nucleoside thiotriphosphates (Sp) to be incorporated into the selection process, [7] which render the resulting aptamers more resistant towards degrading enzymes. Aptamers can also be tested post-SELEX for tolerance of modifications that can further enhance their properties, such as 2'-OMe substitution of purines, 3'capping, and bioconjugation (e.g. with lipids, cholesterol, or polymers).[8] Further, aptamers have been prepared using the enantiomeric form of natural nucleic acids (Spiegelmer"), which makes such aptamers completely unsusceptible to nucleases.<sup>[9]</sup> Together, these advances have considerably addressed the in vivo stability aspect of aptamers, leaving pharmacological limitations a primary hurdle for clinical translation.

We have recently reported that a bottlebrush polymer with dense PEG side chains can enhance the plasma pharmacokinetics (PK) and bioavailability of conjugated antisense oligonucleotides by steric inhibition of specific/non-specific nucleic acid-protein interactions. [10] Such steric selectivity greatly reduces side effects associated with oligonucleotide therapeutics, including coagulopathy and unwanted activation of the immune system. Termed pacD-NA (polymer-assisted compaction of DNA), these nanoscopic bioconjugates produce a novel biodistribution profile, elevate blood circulation times, and augment tissue retention (up to 15 weeks post intravenous injection). These improvements result in massively boosted antisense activities in vivo, with 1–2 orders of magnitude reduction in

Angewandte
International Edition Chemie

dosage requirement in certain cancer xenograft models.<sup>[11]</sup> However, our initial pacDNA system may not be ideal for aptamers due to their tendency to undergo endocytosis, which we speculate stems from the hydrophobic polynorbornene (PN) backbone of the bottlebrush polymer.<sup>[12]</sup> Thus, for applications involving aptamer targeting of extracellular species, a new chemistry that retains the favorable pharmacological properties of prototypical pacDNA but suppresses cellular uptake is preferrable. Herein, we report a novel pacDNA system with a highly hydrophilic, polyphosphodiester backbone capable of extending blood circulation and restoring aptamer bioactivity in vivo.

#### **Results and Discussion**

The polyphosphodiester backbone of the bottlebrush polymer is assembled by stepwise condensation of an Fmocprotected phosphoramidite derived from serinol (Figure 1a and Scheme S1), a common intermediate for pharmaceuticals. Because the synthesis of the polymer backbone shares the same chemistry as oligonucleotide synthesis, the aptamer portion can be prepared as part of the polymer backbone, eliminating subsequent aptamer conjugation and purification steps. For proof of concept, a poly(serinol phosphodiester) (PSP) backbone of 30 repeating units with two dT<sub>15</sub> strands flanking each terminus of the backbone was synthesized (dT<sub>15</sub>-b-PSP<sub>30</sub>-b-dT<sub>15</sub>). Note that the serinol units are racemic. Following the synthesis, the Fmoc groups protecting the serinol amines were removed,

and the strand was purified by reversed-phase high performance liquid chromatography (RP-HPLC, Figure S1).

To construct the bottlebrush segment, the amine groups were derivatized with N-hydroxysuccinimide (NHS)-terminated PEG in a two-stage process. In the first stage, the purified backbone was treated with one equiv. of 10 kDa PEG succinimidyl glutaramide (1:1 amine:NHS ester) in 1× phosphate buffered saline (PBS, pH 7.4) at 4°C overnight. Next, the product from the first stage was lyophilized and reacted with another equiv. of PEG (1:1 amine:NHS ester) in anhydrous N,N-dimethylformamide (DMF) for 60 h at room temperature. The two-stage PEGylation is necessary because NHS esters hydrolyze in an aqueous buffer leading to unsatisfactory coupling efficiencies, but without the initial aqueous coupling step, the anionic backbone/oligonucleotide sequence is insoluble in DMF. With the two-step process, near-quantitative coupling yields (≈95% conversion of serinol amines) were obtained as determined by a 2,4,6trinitrobenzene sulfonic acid (TNBSA) assav using glycine as a standard (Figure S2 and Table S1). The two-stage PEGylation produced incremental increases in molecular weight (MW) after each coupling reaction, as observed by aqueous gel permeation chromatography (GPC) (Figure 1b). Atomic Force Microscopy (AFM) measurement of the final structure,  $dT_{15}$ -b-(PSP<sub>30</sub>-g-PEG)-b- $dT_{15}$  (termed PSP pacDNA) shows a spherical morphology with a drystate diameter of  $21 \pm 3$  nm (Figure 1c and d).

The solid-phase methodology of PSP pacDNA synthesis carries significant advantages over the graft-through approach that we have adopted previously for PN pacDNA.<sup>[14]</sup> For example, the degree of polymerization (DP) can be

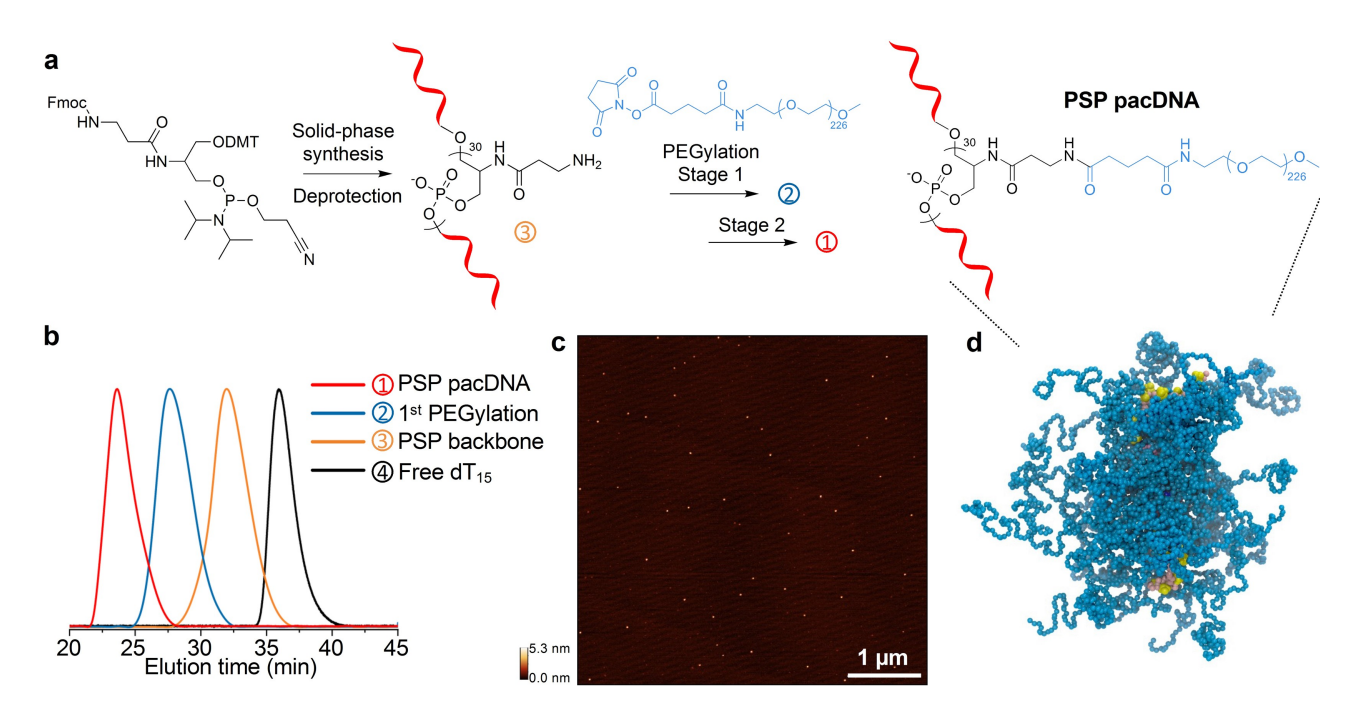


Figure 1. Characterization of PSP pacDNA. a) Schematics of PSP pacDNA synthesis. b) Aqueous GPC chromatograms of PSP pacDNA, intermediate PSP pacDNA after stage 1 PEGylation, PSP backbone, and free dT<sub>15</sub>. c) Representative low-magnification AFM image of PSP pacDNA, showing highly homogeneous, non-aggregating spherical particles. d) The structure of the PSP pacDNA from a coarse-grained molecule dynamics simulation using the MARTINI force field with explicit solvation (blue: PEG; yellow/pink: DNA).

Angewandte
International Edition Chemie

arbitrarily tuned by the number of synthesis cycles. Further, the synthesis provides access to additional molecular architectures, such as branched, dendritic, or block copolymers (or a combination thereof), which can be difficult to achieve with current polymer chemistry.

To test the versatility of our approach, we synthesized PSP bottlebrushes with different backbone DPs ranging from 5 to 35 (a 5' Cy5 was used for quantification). See Tables 1 and S2 for all PSP pacDNA structures and DNA sequences. In addition, we synthesized two architecturally distinct forms of PSP pacDNA: the dumbbell-like pacDNA, where the DNA strand is situated between two bottlebrush segments, and the doubler pacDNA, where the DNA is tethered via the 5' to the middle unit of the brush backbone. The dumbbell-like pacDNA was synthesized with a dT<sub>15</sub> bridge between two PSP<sub>15</sub> segments. For the doubler pacDNA, a dT<sub>15</sub> segment was first synthesized normally (3' to 5'), followed by the addition of a two-way branching unit (doubler phosphoramidite) at the 5', upon which two serinol phosphoramidites were added in each coupling sequence. One benefit for the doubler pacDNA is that the brush

backbone can be synthesized with half of the number of synthesis cycles while achieving the same total number of repeating units. TNBSA assay shows that the number of available amine groups associated with each backbone matches the expected value (Table S1). After the first stage of PEGylation, ≈85% of all backbone amine groups were consumed, and the yield increased to 90-100% after the second stage (Table S1). PSP-backboned bottlebrushes of DP 5, 20, and 35 show an increase in MW and size as evidenced by aqueous GPC (Figure 2a) and dynamic light scattering (DLS) (Figure S3) measurements. Despite the different architectures and insertion positions of dT<sub>15</sub>, PSP pacDNA and the structural variants of similar MW exhibit similar retention times in aqueous GPC (Figure 2b) and hydrodynamic sizes (Figure S3). Narrow polydispersity indices (PDIs) in the range of 1.01-1.11 were observed for all samples. DMF GPC shows slightly higher PDIs in the range of 1.1-1.4 and larger-than-calculated MW, likely due to the polar bottlebrush backbone causing some aggregation in DMF, manifesting in high MW tailing (Figure S4). Both transmission electron microscopy (TEM, Figure S5) and

**Table 1:** Key PSP backbone sequences.

Sample ID	Sequence <sup>[a]</sup>
DP5	5'-Cy5-XXX XXT-3'
DP20	5'-Cy5-XXX XXX XXX XXX XXX XXT-3'
DP35	5'-Cy5-xxx xxx xxx xxx xxx xxx xxx xxx xxx xx
PSP pacDNA	5'-Cy5-TTT TTT TTT TTT TTT XXX XXX XXX XXX XXX
Doubler PSP pacDNA	$(5'$ –XXX XXX XXX XXX XXX) $_2$ D TTT TTT TTT TTT TTT-Cy5–3 $^\prime$
Dumbbell-like PSP pacDNA	5'-Cy5-xxx xxx xxx xxx xxx ttt ttt ttt ttt ttt

[a] X: amine-serinol phosphoramidite; D: symmetric doubler phosphoramidite.

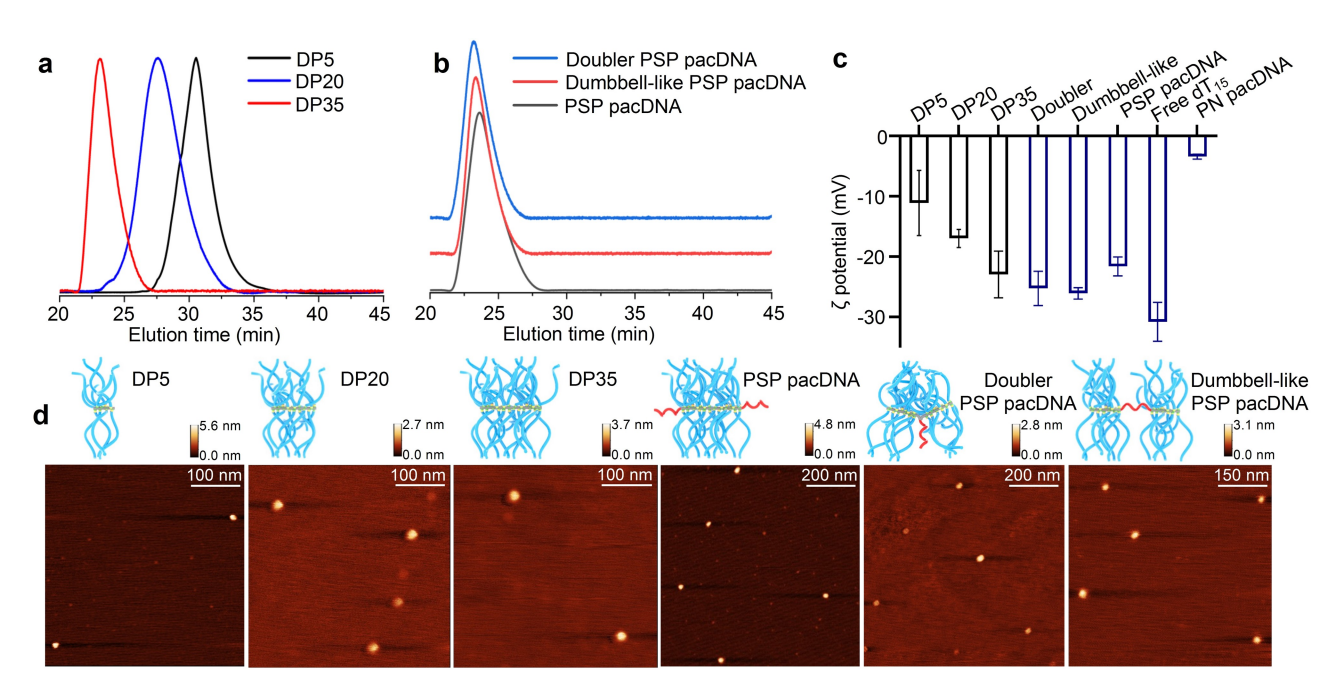


Figure 2. Characterization of various PSP bottlebrushes and pacDNAs. a) Aqueous GPC chromatograms of the PSP bottlebrushes with DPs of 5, 20, and 35. b) Aqueous GPC chromatograms of PSP pacDNAs of various architectures (DNA: dT<sub>15</sub>). c) ζ potential measurements of PSP bottlebrushes, PSP pacDNAs, free dT<sub>15</sub>, and PN pacDNA. d) Representative AFM images of PSP bottlebrushes and PSP pacDNAs.



AFM (Figure 2d and S6) confirm that these molecular brushes are non-aggregating and highly uniform in size in water, and particle size increases with backbone DPs. Consisting of a multitude of phosphodiesters (p $K_a \approx 2.2$ ), PSP bottlebrushes and PSP pacDNAs exhibit negative ζ potentials ranging from -11.1 to -26.1 mV under pH neutral conditions (Nanopure<sup>TM</sup> water) (Figure 2c). Interestingly, PSP pacDNA and a PN-based counterpart of similar MW and hydrodynamic size (Figure S3) exhibit very different ζ potentials: while the PSP materials show highly negative ζ potentials similar to free oligonucleotides, the PN-based material has a near-neutral  $\zeta$  potential. Collectively, these results indicate that the PSP pacDNA synthesis is robust and can be used to prepare molecular brushes containing functional oligonucleotides with a high degree of structural freedom.

The PSP pacDNAs are designed to reduce unwanted oligonucleotide-protein interactions, inhibit non-specific cellular uptake, and prolong blood circulation times. To test the first of these characteristics, we examined the nuclease degradation kinetics of various PSP pacDNAs (Figure S7a). The 3' of dT<sub>15</sub> was labeled with the fluorophore Cy5, and a 5' quencher (dabcyl)-labeled complementary dA<sub>15</sub> strand was hybridized to the PSP pacDNAs. The hybridization kinetics for all PSP pacDNAs were indistinguishable from that of free dT<sub>15</sub>, reaching completion in  $\approx 10$  s. The addition of a non-complementary, quencher-labeled dummy strand did not result in a reduction in Cy5 fluorescence (Figure S7b), ruling out non-specific binding. Upon digestion by the endonuclease DNase I, the fluorophore-quencher pair is separated, leading to an increase of fluorescence. The degradation half-lives of the PSP pacDNAs are roughly three times that of free double-stranded DNA, suggesting some steric shielding effects (Figure S7c and Table S3). In contrast, PEGylation by conventional linear or slightly branched PEG does not alter the degradation half-life by DNase I.[15]

We speculate that a mechanism for the brush-type PEG to enter the cell involves transient adsorption of the polymer onto the plasma membrane (PM), possibly mediated by PEG-cation interactions and the negative PM potential. [16] With PN-based bottlebrushes, the near-neutral  $\zeta$  potential promotes PM adsorption, and the hydrophobic polymer backbone then further increases adhesion strength<sup>[17]</sup> and therefore polymer residence times on the PM, allowing for increased uptake compared with normal PEG or DNA (Figure 3). In contrast, the more negative  $\zeta$  potential and the completely hydrophilic backbone of the PSP pacDNA should reduce the transient polymer-PM interactions and therefore endocytosis. To test this hypothesis, we compared the cellular uptake of a Cy3-labeled PSP pacDNA and a PN-based counterpart by HUVEC (endothelial), NCI-H358 (lung), HEP3B (liver), and SKBR3 (breast) cells using flow cytometry. The results show that the PSP pacDNA consistently undergoes very limited uptake, similar to the levels exhibited by free single-stranded DNA which has been known to exhibit insignificant levels of endocytosis (Figure 4a). [18] Conversely, the PN pacDNA, which has similar MW, architecture, and PEG/DNA content as the PSP

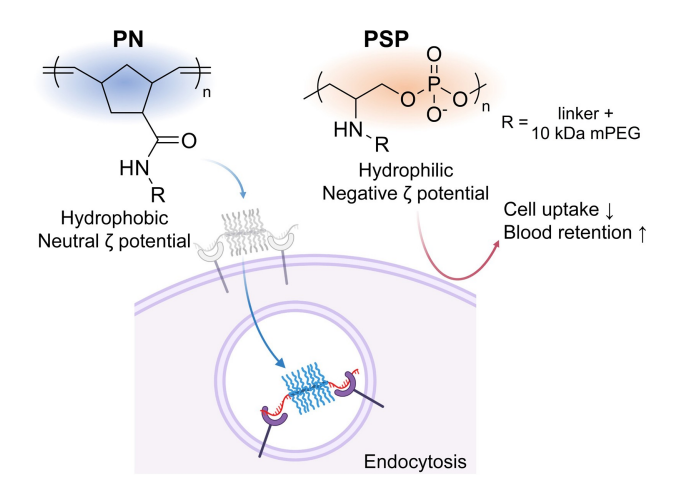


Figure 3. Comparison of the backbone chemistry and cellular uptake of PN- and PSP-based molecular brushes.

pacDNA (Figure S8), shows 6–12 times more rapid cell uptake than PSP pacDNA. These results demonstrate that a small change in the chemical composition of the backbone (no more than 5% in overall MW) can greatly alter the biological characteristics of the bottlebrush polymer.

Persistence in plasma is important to aptamers as rapid clearance can significantly shorten the duration of effect and increase dosage requirements. We hypothesize that PSP pacDNA can improve the plasma PK and the potency of conjugated aptamers by reducing cell uptake levels and avoiding renal clearance. To evaluate the plasma PK, 5'-Cy5-labeled PSP bottlebrushes, PSP pacDNA, and doubler PSP pacDNA were injected into C57BL/6 mice through the tail vein. Blood samples were collected from the submandibular vein at predetermined time points and analyzed using a two-compartment model. Remarkably, the PSP bottlebrushes exhibited very high stability and retention in plasma, with distribution half-lives in the range of 1.6-2.6 h and elimination half-lives between 24 and 35 h (Table S4). There was still > 20% of the injected dose (for DPs=20 and 35) remaining in circulation after 72 h (Figure 4b). For the PSP pacDNA, the plasma clearance is notably faster than the bottlebrushes alone, likely due to degradation of the dT<sub>15</sub> component by plasma nucleases. The doubler PSP pacDNA was cleared slightly faster than the linear counterpart. Still, >10% of both PSP pacDNAs was found within the plasma 24 h post-injection, while there was <1% free  $dT_{15}$  in circulation after only 2 h and < 0.1 % after 24 h. Estimating bioavailability by calculating the area under the curve (AUC<sub>∞</sub>), PSP pacDNA are 15-25 times more bioavailable than free  $dT_{15}$  (Table S4).

To follow the bottlebrush component of the PSP pacDNA in vivo for an extended period of time and investigate its biodistribution, SKH1-Elite mice, an immuno-competent hairless strain, were injected with a 5'-Cy5-labeled PSP bottlebrush with a DP of 30 via the tail vein. Live animal imaging showed that fluorescence gradually increased near the skin of the mice, reaching peak levels after 48 h. The fluorescence persisted at peak levels until

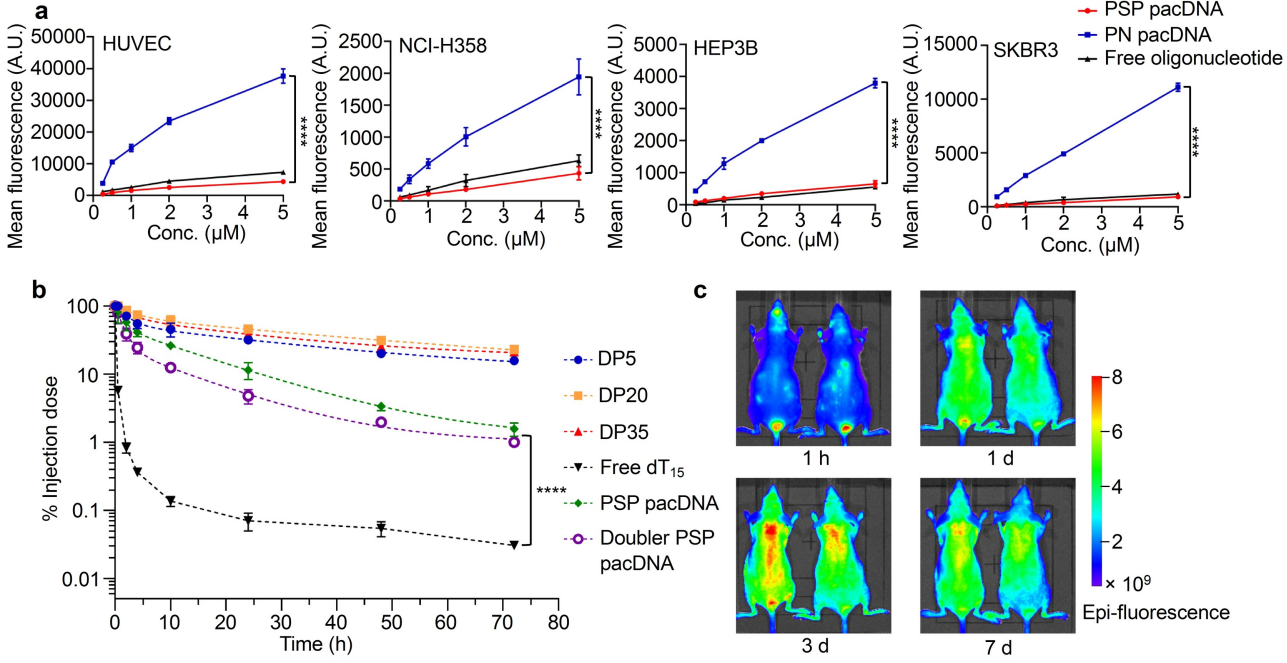


Figure 4. In vitro and in vivo characterization of PSP bottlebrushes and pacDNAs. a) Cellular uptake of PSP pacDNA, PN pacDNA, and free oligonucleotide by HUVEC, NCI-H358, HEP3B, and SKBR3 cells. b) Plasma pharmacokinetics of PSP pacDNA, doubler PSP pacDNA, PSP bottlebrushes, and free dT<sub>15</sub>. c) Fluorescence imaging of SKH1-Elite mice following i.v. injection of Cy5-labeled PSP bottlebrush with a DP of 30. Statistical significance was calculated using two-way ANOVA. \*\*\*\* P < 0.0001.

approximately the 7<sup>th</sup> day post injection (Figure 4c and S9), before slowly decreasing to slightly above-background levels in five weeks. On days 3, 7, and 37, animals were euthanized, and major organs were excised for imaging. All major internal organs (bar the brain) as well as muscle exhibited uptake without a strong preference for any organ. However, interestingly, pronounced accumulation in the skin (including epidermis, dermis, and the skin-draining lymph nodes) was observed. The skin was also the only organ to continue to exhibit fluorescence on day 37 (Figure S10). In immunodeficient athymic nude mice, which lack T cells, a similar observation was made (Figure S11). The skin accumulation of PSP pacDNA may be due to the characteristics of the terminal networks of blood supply capillaries and/or the eventual uptake of the PSP pacDNA by skin-resident immune cells, such as dendritic cells, macrophages, and mast cells.[19] Additional studies are required to elucidate the underlying mechanism for this phenomenon.

To demonstrate the binding efficacy of PSP pacDNA containing a functional aptamer, we adopted a thrombinbinding aptamer, HD1, as a model system. HD1 is a 15nucleotide DNA sequence folding into an antiparallel Gquadruplex that can specifically bind to the exosite I of human alpha thrombin (Table S1).[20] Upon binding, HD1 can inhibit the coagulation and prolong coagulating times. [21] Having a dissociation constant  $(k_d)$  in the nanomolar range, HD1 has been envisioned as a short-term anticoagulant that can be used intraoperatively to reduce the risk of thromboembolism.<sup>[22]</sup> Several studies have demonstrated improved ex vivo efficacy of HD1 through polymeric micelles or DNA origami.[23] However, in vivo potency of HD1 has not been robustly demonstrated. We first assessed the binding affinity of HD1 and the corresponding pacDNA (PSP pacHD1) by microscale thermophoresis (MST) using Cy5-labeled human alpha thrombin as the target. It was found that the appendage of the bottlebrush structure to HD1 has a nominal impact on its binding affinity, with the  $k_{\rm d}$  of free HD1 and PSP pacHD1 being 5.4 nM and 6.9 nM, respectively. In addition, a PSP pacDNA containing a scrambled sequence (PSP pacSCR) exhibited no measurable binding with thrombin, ruling out the bottlebrush component being responsible for the observed binding (Figure 5a). Next, we evaluated the anticoagulation properties of HD1 and PSP pacHD1 in human plasma by measuring the prothrombin time (PT) and activated partial thromboplastin time (aPTT) (Figure 5b and c). Interestingly, while free HD1 induced a more pronounced effect in the PT assay, the PSP pacHD1 was more effective in the aPTT assay, with almost three-fold longer coagulating times compared to the vehicle. One interpretation for this difference is that the intrinsic/extrinsic pathways of the coagulation cascade are affected differently by the test agents. Again, PSP pacSCR did not show anticoagulation effects. Importantly, the anticoagulation was completely reversible through the use of a locked nucleic acid (LNA)-based antidote that consists of a fully complementary strand to HD1, which disrupts its secondary structure.[24] Such an antidote would be an invaluable tool for the perioperative management of patients receiving anticoagulants. Interestingly, although developed as a human thrombin binder, HD1 can also cause prolonged coagulation in mouse plasma, and the strengths of the effect were found to be comparable in both species. 5213773, 2022, 41, Downloaded from https://onlinelbrary.wiley.com/doi/10.1002/anie.202204576 by Northeaser University. Wiley Online Library on [31/03/2023]. See the Terms and Conditions (https://onlinelibrary.wiley.com/terms-and-conditions) on Wiley Online Library or rules of use; OA articles are governed by the applicable Creative Commons Licensea

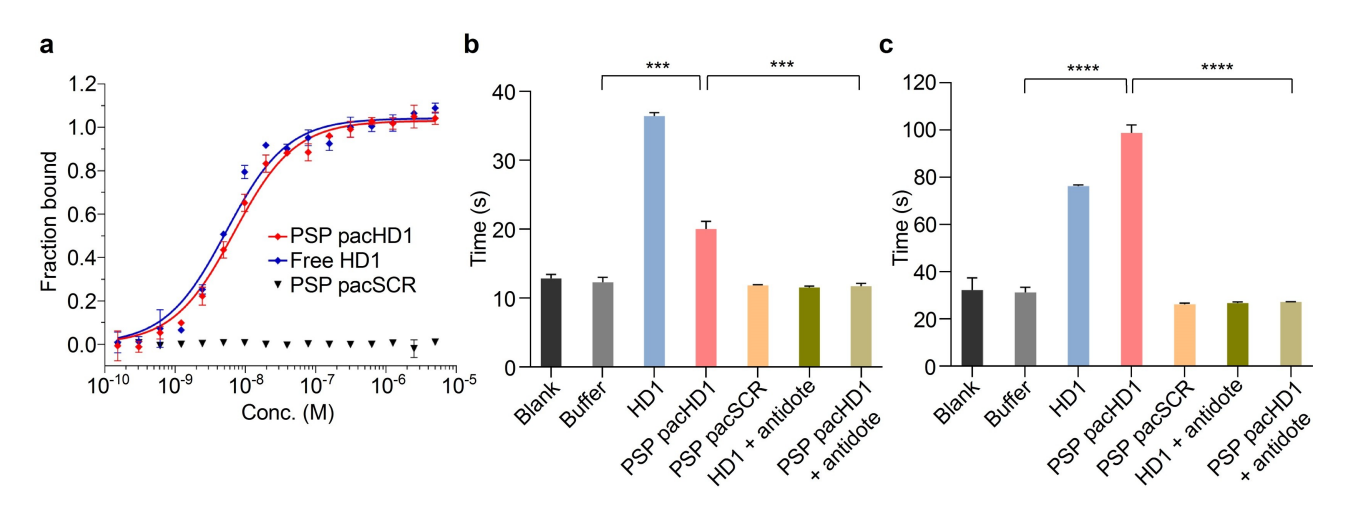


Figure 5. Binding affinity and anticoagulation test in human plasma. a) Binding analysis of free HD1, PSP pacHD1, and PSP pacSCR measured by MST. b) PT measurements of human plasma treated with samples and controls (5 µM). c) aPTT measurements of human plasma treated with samples and controls (5 μM). Statistical significance was calculated using Student's two-tailed t test. \*\*\* P < 0.001, \*\*\*\* P < 0.0001.

Furthermore, the diverging relative strengths of HD1 and PSP pacHD1 in PT and aPTT assays were also observed in mouse plasma (Figure 6a and b).

The complex and dynamic in vivo environment represents the ultimate challenge for aptamers. To assess the ability of the PSP pacDNA to serve as an aptamer enhancer in vivo, free HD1 and the PSP pacHD1 were injected in vivo in C57BL/6 mice. Plasma PK measurements of 5'-Cy5labeled materials reveal that the PSP pacHD1 persists in the blood markedly longer than free HD1, with a 16-fold difference in AUC (Figure 6c). Interestingly, placing the Cy5 at the 5' of PSP pacDNA results in slightly better blood retention than placement at the 3' (see Figure S12 for PK parameters). The difference may be due to the fact oligonucleotide degradation in plasma (both mouse and human) occurs primarily by 3'-to-5' exonucleolytic activity. [25] When analyzing anticoagulating properties, it was found that free HD1 produced no statistically significant difference compared to blank in both PT and aPTT assays using blood collected 5 min after injection, although in purified plasma HD1 does exhibit potency (see above). The rapid and complete loss of activity of free HD1 in vivo may be attributed to a combination of degradation, non-specific binding, and rapid renal clearance. In stark contrast, the PSP pacHD1 exhibited a 3-fold increase in PT and a 5-fold increase in aPTT measurements relative to blank (Figure 6d and e). The effect attenuates slowly, reaching baseline levels in  $\approx 2$  h. When a dose of the LNA antidote (10 equiv to HD1) was delivered i.v. 20 min after the administration of PSP pacHD1, the anticoagulating effect was completely neutralized in the next blood collection timepoint (30 min). Comparing the PSP pacHD1 to its PN-based counterpart, it can be seen that the PN pacHD1 produced <50% of the effect as the PSP pacHD1 at the 5 min timepoint, although both types of polymers exhibit similar plasma PK,[12] which highlights the importance of the phosphodiester backbone of the PSP pacDNA. The in vivo anticoagulatory effect of PSP pacHD1 was further quantified using a murine tailtransection bleeding model (Figure 6f). Shortly (5 min) after receiving the test agents and controls, the tails of mice were clipped and blood from the tail was collected for 15 min. Treatment with PSP pacHD1 induced the largest amount of blood loss (76 µL), while free HD1- and vehicle-treated mice lost 26 µL and 16 µL blood, respectively. When mice were given PSP pacHD1 and the LNA antidote sequentially, tail bleeding reverted to the baseline rate. Taken together, these results demonstrate that the PSP pacDNA structure considerably enhances the plasma PK, bioavailability, and the potency of the conjugated aptamer, and the activity is controllable using an antidote.

The PSP pacHD1 was found to be non-cytotoxic up to 5 μM for NCI-H358 cells (Figure S13). However, free HD1 exhibits slight inhibition of cell growth, possibly due to nonspecific binding to cell surface receptors leading to erroneous signaling. Activation of the immune system by PSP pacHD1 was investigated by analyzing complement C3 and selected cytokines in C57BL/6 mice following systemic delivery. The treatment with PSP pacHD1, PN pacHD1, and free HD1 resulted in no significant change in C3 levels relative to PBS control (Figure S14). Tumor necrosis factor- $\alpha$  (TNF- $\alpha$ ) and interleukin 6 (IL-6) exhibited statistically significant activation for the PSP pacHD1 group compared to PBS control, but the activation is weak. IL-12 levels showed no obvious changes. In contrast, lipopolysaccharide (LPS, positive control), induced strong expression of all three cytokines. These results are consistent with our previous finding that the bottlebrush architecture makes the conjugate uniquely non-immunogenic (even for the PEG component), while the conventional, linear PEG-DNA conjugate can elicit both innate and adaptive immune responses.<sup>[11]</sup> Collectively, these data suggest that the PSP pacHD1 is generally safe without major acute toxic or immunological shortcomings.



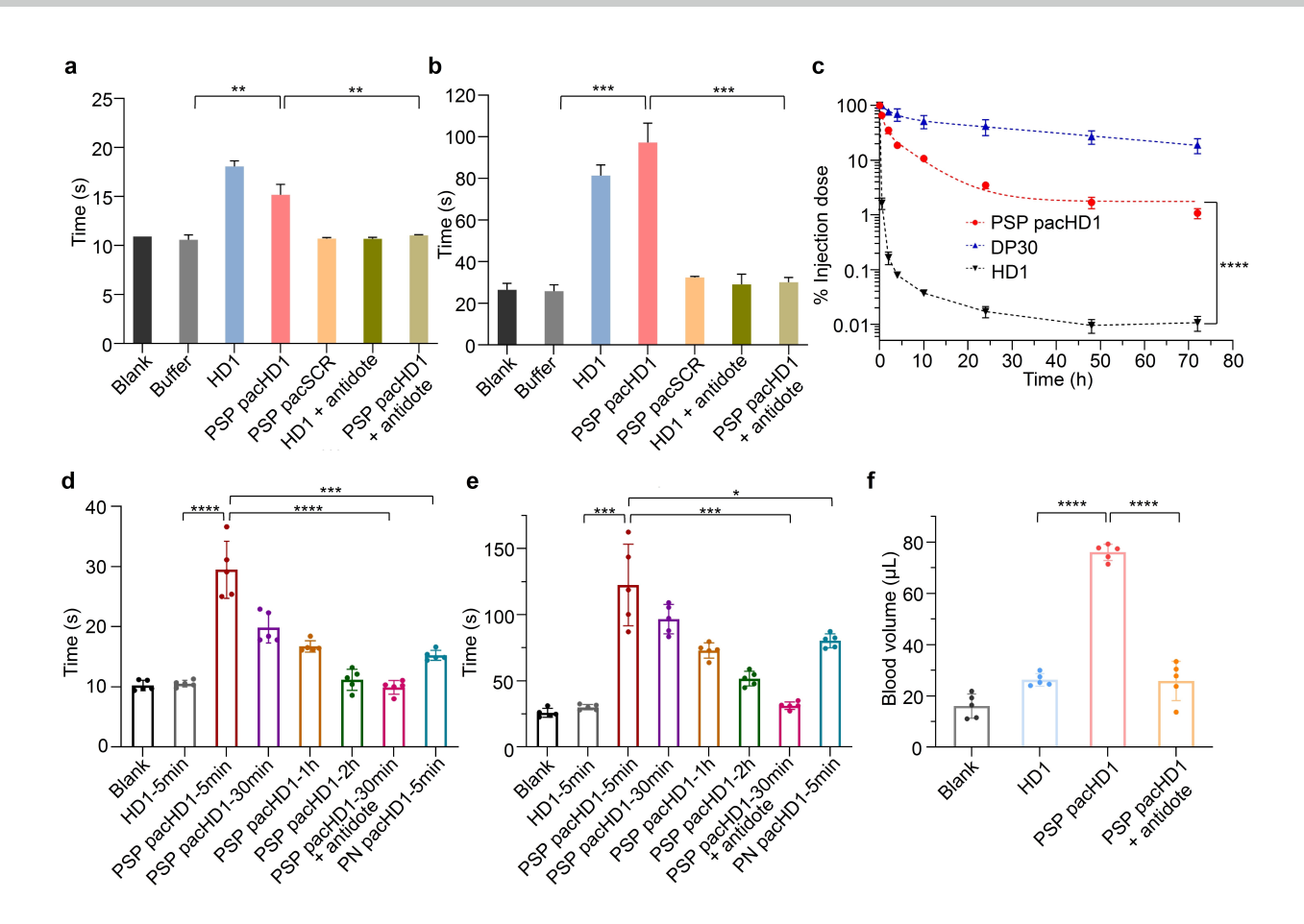


Figure 6. Anticoagulation by PSP pacHD1 in mouse plasma and in vivo. Measurements of PT (a) and aPTT (b) of mouse plasma (ex vivo) treated with samples and controls (5  $\mu$ M). Statistical significance was calculated using Student's two-tailed t test. \*\*P<0.01, \*\*\*\*P<0.001. c) Plasma pharmacokinetics of free HD1, PSP pacHD1 and PSP bottlebrush (DP30). Statistical significance was calculated using two-way ANOVA. \*\*\*\*P<0.0001. Measurements of PT (d) and aPTT (e) of mouse plasma withdrawn at predetermined time points after in vivo injection of samples and controls in C57BL/6 mice. f) Tail transection bleeding test of C57BL/6 mice after being treated in vivo with samples and controls. Statistical significance was calculated using Student's two-tailed t test. \*P<0.1, \*\*\*\*P<0.001, \*\*\*\*P<0.0001.

## Conclusion

In summary, we have developed a facile route to a novel bottlebrush polymer that can be used to enhance the pharmacological properties and in vivo performance of aptamers. Termed PSP pacDNA, the unimolecular polymeroligonucleotide biohybrid can be synthesized in the same step as the therapeutic sequence via the automated solidphase methodology, followed by near-quantitative PEGylation. The synthesis is highly versatile with regard to the size and architecture of the final polymer and does not involve heavy metal catalysts that can complicate downstream applications. Importantly, the PSP pacDNA consists only of building blocks that are recognized as safe in pharmaceutical applications, and does not involve a non-degradable, longchain aliphatic backbone. The hydrophilic phosphodiester backbone of the PSP pacDNA resists cellular uptake, and the spatially congested PEG environment reduces nonspecific binding, leading to elevated blood retention times and increased productive binding. These properties impart the PSP pacDNA superior performance in an anticoagulation mouse model compared to the free aptamer, which exhibits potency in vitro but no activity in vivo. Of note, the aptamer we adopted is not chemically modified, making it susceptible to degrading nucleases. We envision that, with advanced, chemically stabilized aptamer variants, it is possible to design PSP pacDNA having antibody-like in vivo potency and durability but with all the benefits associated with aptamers.

### Acknowledgements

This work was supported by the National Institute of General Medical Sciences (1R01GM121612), the National Cancer Institute (1R01CA251730), and the National Science Foundation (DMR award number 2004947). We thank Prof. Meni Wanunu for the use of AFM, Prof. Ambika Bajpayee for the help on MST, Prof. Jiahe Li for the use of flow cytometer and Prof. Heather Clark for the use of in vivo imaging system. We also thank the Institute for Chemical Imaging of Living System at Northeastern University for





instrument support. S.S.D. would like to thank Northeastern University for the startup funding and Northeastern University Research Computing for the computing resources.

#### **Conflict of Interest**

The authors declare no conflict of interest.

### **Data Availability Statement**

The data that support the findings of this study are available in the Supporting Information of this article.

**Keywords:** Anticoagulant · Aptamer · Bottlebrush Polymer · Oligonucleotides · PEGylation

- [1] A. D. Keefe, S. Pai, A. Ellington, *Nat. Rev. Drug Discovery* **2010**, *9*, 537–550.
- **2010**, 9, 537–550. [2] J. Zhou, J. Rossi, *Nat. Rev. Drug Discovery* **2017**, *16*, 181–202.
- [3] a) K. D. Kovacevic, J. C. Gilbert, B. Jilma, Adv. Drug Delivery Rev. 2018, 134, 36–50; b) A. Lacroix, H. F. Sleiman, ACS Nano 2021, 15, 3631–3645; c) Y.-H. Lao, K. K. L. Phua, K. W. Leong, ACS Nano 2015, 9, 2235–2254; d) M. R. Dunn, R. M. Jimenez, J. C. Chaput, Nat. Chem. Rev. 2017, 1, 0076.
- [4] E. W. M. Ng, D. T. Shima, P. Calias, E. T. Cunningham, D. R. Guyer, A. P. Adamis, *Nat. Rev. Drug Discovery* 2006, 5, 123–132.
- [5] E. Akyol, A. Lotery, Biologics 2020, 14, 83-94.
- [6] a) A. D. Ellington, J. W. Szostak, *Nature* 1990, 346, 818–822;
   b) C. Tuerk, L. Gold, *Science* 1990, 249, 505–510.
- [7] H. Aurup, D. M. Williams, F. Eckstein, *Biochemistry* 1992, 31, 9636–9641.
- [8] a) X. Tao, X. Wang, B. Liu, J. Liu, Biosens. Bioelectron. 2020, 168, 112537; b) Z. Geng, L. Wang, K. Liu, J. Liu, W. Tan, Angew. Chem. Int. Ed. 2021, 60, 15459–15465; Angew. Chem.
  2021, 133, 15587–15593; c) S. Hong, X. Zhang, R. J. Lake, G. T. Pawel, Z. Guo, R. Pei, Y. Lu, Chem. Sci. 2020, 11, 713–720; d) L. Wu, Y. Wang, X. Xu, Y. Liu, B. Lin, M. Zhang, J. Zhang, S. Wan, C. Yang, W. Tan, Chem. Rev. 2021, 121, 12035–12105; e) S. Ni, Z. Zhuo, Y. Pan, Y. Yu, F. Li, J. Liu, L. Wang, X. Wu, D. Li, Y. Wan, L. Zhang, Z. Yang, B.-T. Zhang, A. Lu, G. Zhang, ACS Appl. Mater. Interfaces 2021, 13, 9500–9519.
- [9] a) S. Klußmann, A. Nolte, R. Bald, V. A. Erdmann, J. P. Fürste, *Nat. Biotechnol.* 1996, 14, 1112–1115; b) A. Vater, S. Klussmann, *Drug Discovery Today* 2015, 20, 147–155.
- [10] a) F. Jia, X. Lu, X. Tan, D. Wang, X. Cao, K. Zhang, Angew. Chem. Int. Ed. 2017, 56, 1239–1243; Angew. Chem. 2017, 129, 1259–1263; b) X. Lu, T.-H. Tran, F. Jia, X. Tan, S. Davis, S.

- Krishnan, M. M. Amiji, K. Zhang, J. Am. Chem. Soc. 2015, 137, 12466–12469.
- [11] D. Wang, Q. Wang, Y. Wang, P. Chen, X. Lu, F. Jia, Y. Sun, T. Sun, L. Zhang, F. Che, J. He, L. Lian, G. Morano, M. Shen, M. Ren, S. Dong, J. J. Zhao, K. Zhang, *Proc. Natl. Acad. Sci. USA* 2022, 119, e2113180119.
- [12] D. Wang, J. Lin, F. Jia, X. Tan, Y. Wang, X. Sun, X. Cao, F. Che, H. Lu, X. Gao, J. C. Shimkonis, Z. Nyoni, X. Lu, K. Zhang, Sci. Adv. 2019, 5, eaav9322.
- [13] B. Andreeßen, A. Steinbüchel, AMB Express 2011, 1, 12–12.
- [14] L. Charles, J.-F. Lutz, Acc. Chem. Res. 2021, 54, 1791–1800.
- [15] X. Lu, F. Jia, X. Tan, D. Wang, X. Cao, J. Zheng, K. Zhang, J. Am. Chem. Soc. 2016, 138, 9097–9100.
- [16] a) D. Yu, Y. Zhao, Y. H. Choe, Q. Zhao, M. C. Hsieh, P. Peng, Cancer Res. 2004, 64, 149; b) M. G. Schrlau, N. J. Dun, H. H. Bau, ACS Nano 2009, 3, 563–568; c) A. Magarkar, E. Karakas, M. Stepniewski, T. Róg, A. Bunker, J. Phys. Chem. B 2012, 116, 4212–4219; d) I. F. Hakem, J. Lal, M. R. Bockstaller, Macromolecules 2004, 37, 8431–8440.
- [17] a) A. K. Pearce, R. K. O'Reilly, *Biomacromolecules* 2021, 22, 4459–4469; b) C.-F. Su, H. Merlitz, H. Rabbel, J.-U. Sommer, *J. Phys. Chem. Lett.* 2017, 8, 4069–4076.
- [18] R. L. Juliano, X. Ming, K. Carver, B. Laing, *Nucleic Acid Ther.* 2014, 24, 101–113.
- [19] E. A. Sykes, Q. Dai, K. M. Tsoi, D. M. Hwang, W. C. W. Chan, Nat. Commun. 2014, 5, 3796.
- [20] a) L. C. Bock, L. C. Griffin, J. A. Latham, E. H. Vermaas, J. J. Toole, *Nature* 1992, 355, 564–566; b) L. R. Paborsky, S. N. McCurdy, L. C. Griffin, J. J. Toole, L. L. Leung, *J. Biol. Chem.* 1993, 268, 20808–20811.
- [21] C. A. Kretz, A. R. Stafford, J. C. Fredenburgh, J. I. Weitz, J. Biol. Chem. 2006, 281, 37477–37485.
- [22] a) C. Riccardi, E. Napolitano, C. Platella, D. Musumeci, D. Montesarchio, *Pharmacol. Ther.* 2021, 217, 107649; b) K. Derszniak, K. Przyborowski, K. Matyjaszczyk, M. Moorlag, B. de Laat, M. Nowakowska, S. Chlopicki, *Front. Pharmacol.* 2019, 10, 68.
- [23] a) A. Roloff, A. S. Carlini, C. E. Callmann, N. C. Gianneschi, J. Am. Chem. Soc. 2017, 139, 16442–16445; b) S. Zhao, R. Tian, J. Wu, S. Liu, Y. Wang, M. Wen, Y. Shang, Q. Liu, Y. Li, Y. Guo, Z. Wang, T. Wang, Y. Zhao, H. Zhao, H. Cao, Y. Su, J. Sun, Q. Jiang, B. Ding, Nat. Commun. 2021, 12, 358.
- [24] a) C. P. Rusconi, J. D. Roberts, G. A. Pitoc, S. M. Nimjee, R. R. White, G. Quick, E. Scardino, W. P. Fay, B. A. Sullenger, Nat. Biotechnol. 2004, 22, 1423–1428; b) C. P. Rusconi, E. Scardino, J. Layzer, G. A. Pitoc, T. L. Ortel, D. Monroe, B. A. Sullenger, Nature 2002, 419, 90–94.
- [25] P. S. Eder, R. J. DeVine, J. M. Dagle, J. A. Walder, *Antisense Res. Dev.* 1991, 1, 141–151.

Manuscript received: March 28, 2022 Accepted manuscript online: August 18, 2022 Version of record online: September 6, 2022